targets

MDPI

Article

A Dual-Aptamer Electrochemical Sensor for Simultaneous Detection of L-Lactate and Prostate-Specific Antigen

Ziheng Hu [1], Xiaoqian Zhou [1], Haicheng Song [1], Fuliang Wei [1], Zhenzhen Li [1,*] and Lingyan Feng [1,2,*]

[1] Materials Genome Institute and Shanghai Engineering Research Center of Organ Repair, Shanghai University, 99 Shangda Road, Shanghai 200444, China; zihenghu@shu.edu.cn (Z.H.); xq_zhou1999@163.com (X.Z.); shc0725@shu.edu.cn (H.S.); weifuliang@shu.edu.cn (F.W.)

[2] QianWeichang College, Shanghai University, 99 Shangda Road, Shanghai 200444, China

* Correspondence: zhenzhen_li@shu.edu.cn (Z.L.); lingyanfeng@t.shu.edu.cn (L.F.); Tel.: +86-21-66136189 (L.F.)

Abstract

Accurate analysis of prostate cancer (PC)-related biomarkers requires sensing platforms capable of sensitive and multiplex detection in complex biological environments. Herein, we propose a signal-on electrochemical aptamer-based sensor (E-AB) for the simultaneous detection of L-lactate (L-Lac) and prostate-specific antigen (PSA). To maximize analytical performance, two Lac aptamer sensing configurations, single-stranded (ssLac201) and double-stranded (dsLac201), were constructed and comparatively evaluated. The dsLac201 structure displayed more effective background suppression and enhanced target induced signal response. Under optimized conditions, the dsLac201-based sensor exhibited a wide linear range from 500 nM to 10 mM for L-Lac, with a low detection limit of 157 nM and high selectivity. Based on this optimized design, a dual-aptamer electrochemical platform was further engineered through programmable nucleic acid assembly, enabling simultaneous detection of L-Lac and PSA via dual-input signal integration. The dual-target sensor showed broad analytical ranges for both biomarkers (L-Lac: 500 nM–10 mM; PSA: 10 pg mL^{-1}–500 ng mL^{-1}) and retained promising performance in serum samples. This work demonstrates a simple and versatile strategy for multiplex electrochemical biosensing and provides a promising platform for PC-related biomarker monitoring and clinical biomedical analysis.

Keywords: aptamer; biomarkers; PSA; lactate; electrochemical biosensor; dual target detection

1. Introduction

Prostate cancer (PC) is the second most commonly diagnosed malignancy in men worldwide and represents a significant global health challenge [1]. In China, both the incidence and mortality of PC have increased steadily in recent years. Despite the fact that the 5-year survival rate exceeds 99% for patients diagnosed at an early stage, PC often progresses silently due to the lack of obvious early symptoms, resulting in many patients being diagnosed at intermediate or advanced stages. In particular, the 5-year survival rate for metastatic PC declines to approximately 31%, and disease recurrence remains a major challenge even following surgical intervention [2,3]. Therefore, it is critical to develop effective strategies for early detection and prognostic evaluation of PC. Currently, prostate-specific antigen (PSA) is the most widely used biomarker for the early diagnosis of PC and for monitoring disease recurrence after treatment [4,5]. PSA is an androgen-regulated serine protease (33–34 kDa) belonging to the kallikrein protein family, and it is mainly

Academic Editors: Andreas Tsakalof and Ioannis Kanakis

Received: 24 March 2026
Revised: 27 April 2026
Accepted: 29 April 2026
Published: 2 May 2026

secreted by epithelial cells in the prostate acini and ducts [6]. Increased serum PSA levels are commonly used as an indicator of prostate abnormalities. A serum PSA concentration above 4.0 ng/mL is generally considered suggestive of potential PC, while levels exceeding 10 ng/mL are often regarded as highly indicative of prostate malignancy [7]. However, PSA-based screening suffers from limited diagnostic specificity and sensitivity, as elevated PSA levels may also occur in benign conditions such as prostatitis or prostatic hyperplasia. Consequently, reliance on PSA alone can lead to false-positive and false-negative results, which may cause unnecessary biopsies and increase the clinical and psychological burden on patients [8]. Therefore, the development of multi-target detection approaches has attracted increasing attention as a promising strategy to improve the accuracy and reliability of PC diagnosis.

Lactic acid (Lac) is a key metabolic intermediate involved in cellular energy metabolism. Under hypoxic conditions, D-glucose is converted into L-Lac through anaerobic glycolysis, a metabolic pathway that is frequently upregulated in tumor cells [9]. Under normal physiological conditions, the concentration of L-Lac in human blood typically ranges from 0.5 to 2.2 mM [10]. However, studies using high-resolution magic-angle spinning (HR-MAS) spectroscopy have revealed that Lac levels are significantly elevated in PC tissues compared with those in normal prostate tissues [11]. Moreover, increasing evidence indicates that Lac accumulation is closely associated with tumor progression and malignancy grade [12]. In advanced cases of PC, Lac concentrations may rise dramatically, with levels approaching 10 mM, which has been linked to the development of lactic acidosis in cancer patients [13]. These findings suggest that Lac not only reflects metabolic reprogramming in tumor cells but also can serve as a promising complementary biomarker to PSA, thereby providing additional information to improve the accuracy of PC diagnosis.

A variety of analytical methods have been developed for the detection of PSA and Lac. Conventional analytical techniques, including high-performance liquid chromatography (HPLC) and gas chromatography-mass spectrometry (GC-MS), provide accurate and reproducible quantitative results [14,15]. Despite their high analytical performance, these methods require costly instrumentation, laborious sample preparation, and skilled technical personnel, which significantly restrict their wide applications. Electrochemical sensing technologies have attracted much attention in biomedical diagnosis due to their high sensitivity, fast response, portability, and relatively low cost [16]. Compared with conventional analytical techniques, electrochemical methods offer significant advantages, including simple instrumentation, minimal sample preparation, and the potential for miniaturization and on-site analysis, making them highly suitable for clinical diagnostics and point-of-care testing [17].

Among various biosensing strategies, electrochemical aptamer-based (E-AB) biosensors have emerged as a promising platform for biomarkers detection [18]. Aptamers are short single-stranded DNA or RNA oligonucleotides selected through the systematic evolution of ligands by exponential enrichment (SELEX) process, which enables them to bind specifically and strongly to a wide range of targets, including proteins, small molecules, and cells [19]. Compared with traditional antibodies, aptamers offer several advantages, such as high binding affinity, good chemical stability, easy synthesis and modification, and low batch-to-batch variation [20]. By integrating aptamers with electrochemical transduction systems, E-AB biosensors can convert target-recognition events into measurable electrical signals [21,22]. These sensors typically rely on target-induced conformational changes in the aptamer and distance-dependent electron-transfer processes, enabling sensitive and selective detection of analytes. Due to their high sensitivity, excellent selectivity, and operational simplicity, E-AB sensors have become powerful analytical tools for the detection of a wide range of biomarkers and small molecules [23,24]. Furthermore, the inherent

programmability of nucleic acid aptamer sequences can facilitate rational structure design, enabling the construction of multiplexed sensing platforms for simultaneous multi-target detection [25–28].

Herein, we developed a "signal-on" electrochemical sensing strategy for the detection of L-Lac and PSA. The used aptamers against Lac and PSA were adopted from previously reported studies with reported binding affinity (K_d) of 0.43 mM and 40 nM, respectively [10,29]. To improve analytical performance, two aptamer sensing configurations for Lac detection, namely single-stranded (ssLac201) and double-stranded (dsLac201) probes, were first designed and systematically evaluated using differential pulse voltammetry (DPV). The dsLac201-based sensor exhibited higher signal response and effectively suppressed background noise compared with the ssLac201 probe. Utilizing the optimized dsLac201 sensing probe, a dual-target detection platform was further constructed by integrating L-Lac and PSA aptamers through an "AND" logic gate design. The proposed sensor enabled simultaneous and sensitive detection of both biomarkers, offering a promising approach for enhancing the accuracy of PC diagnosis and monitoring tumor-associated metabolic changes.

2. Experimental Section

2.1. Materials and Reagents

The oligonucleotides used in this work were synthesized and HPLC-purified by Sangon Biotech Co., Ltd. (Shanghai, China), the detailed sequences are listed in Table 1. 4-(2-hydroxyethyl) piperazine-1-ethanesulfonic acid (HEPES), tris-(2-carboxyethyl) phosphine hydrochloride (TCEP), 6-mercapto-1-hexanol (MCH), potassium ferricyanide ($K_3Fe(CN)_6$), potassium ferrocyanide trihydrate ($K_4Fe(CN)_6 \cdot H_2O$), L-lactic acid, D-lactic acid, glycine, L-alanine, L-cysteine, and acetic acid were purchased from Aladdin Reagent Co., Ltd. (Shanghai, China). Sodium chloride (NaCl) was obtained from Sigma-Aldrich (Shanghai, China). Glucose, sodium hydroxide (NaOH), potassium chloride (KCl), and magnesium chloride ($MgCl_2$) were purchased from Sinopharm Chemical Reagent Co., Ltd. (Shanghai, China). Fetal bovine serum (FBS) was acquired from Sangon Biotech Co., Ltd. (Shanghai, China). All reagents were analytical grade and used without further purification. Ultra-pure water (18 MΩ, Milli-Q, Millipore, Burlington, MA, USA) was used throughout all experiments.

Table 1. The sequences of used oligonucleotides.

Name	Sequence (5′-3′)
Lac201	SH-GAC GAC GAG TAG CGC GTA TGA ATG CTT TTC TAT GGA GTC GTC-Fc
cDNA	AGT CGT CGA GAG
Lac201-anti-PSA	SH-AGC TTT AAT GAC GAC GAG TAG CGC GTA TGA ATG CTT TTC TAT GGA GTC GTC-Fc
PSA-apt	ACT CGT CGT CAT TAA AGC TCG CCA TCA AAT AGC TGC

2.2. Electrode Cleaning

Prior to aptamer modification, the bare gold electrodes (AuE, ø 2 mm) were polished with 0.3 and 0.05 μm alumina powder, followed by sonication in Milli-Q water to remove residual polishing agent. Subsequently, the electrodes were electrochemically cleaned following a previously established protocol [30]. Briefly, electrochemical treatment of the polished AuE was conducted as follows:(1) Cyclic voltammetry (CV) scanning was performed in 0.5 M NaOH solution with a potential range of −0.35 V to −1.35 V at a scan rate of 2 V/s, repeated 1000 times;(2) CV scanning was performed in 0.5 M H_2SO_4 solution with a potential range of −0.35 V to 1.5 V at a scan rate of 1 V/s, repeated 100 times.

The active electrode area was obtained from CV scans performed in 0.05 M H_2SO_4 at a scan rate of 0.1 V/s. The effective surface area of the electrode was calculated by integrating the charge of the gold reduction peak.

2.3. Preparation of the Sensor

Before surface modification, the disulfide-modified Lac201 aptamer was reduced with 10 mM TCEP for 1 h. To prepare the double-stranded structure (dsLac201), the Lac201 aptamer and its complementary DNA (cDNA) were mixed, heated at 95 °C for 5 min, and slowly cooled to 25 °C. The treated aptamer solution was then diluted with 50 mM HEPES buffer to the desired concentrations. Then, 5 µL of the aptamer solution was dropped onto the cleaned AuE surface and incubated for 12 h in the dark to facilitate the formation of a self-assembled monolayer via thiol-gold covalent bonding. Following aptamer immobilization, the AuE was immersed in 10 mM MCH for 30 min to block non-specific active sites. Finally, the electrode was rinsed with ultra-pure water and HEPES buffer to remove physically adsorbed residues. The fabricated sensor was stored in HEPES buffer prior to the measurements. For Lac detection, the modified electrode was incubated with varying concentrations of Lac prior to electrochemical measurements.

To construct the dual-aptamer electrochemical sensor, the extended Lac aptamer (Lac201-anti-PSA) was first hybridized with the PSA aptamer through partial complementary base pairing. Briefly, Lac201-anti-PSA and PSA aptamer were mixed at same concentration in HEPES buffer, heated to 95 °C for 5 min, and then slowly cooled to room temperature to form a stable duplex structure. The subsequent immobilization procedures were same as described above.

2.4. Electrochemical Measurements

All electrochemical data were obtained from an Autolab potentiostat/galvanostat PGSTAT302 (Metrohm AG, Herisau, Switzerland) with a three-electrode system at room temperature, including a AuE working electrode, saturated Ag/AgCl reference electrode and a platinum wire counter electrode. DPV measurements were performed in 50 mM HEPES buffer via potential scans between 0 and 0.7 V and step potential 0.01 V, modulation amplitude 0.025 V, modulation time 0.05 s. CV measurements were recorded in a potential window ranging from −0.2 V to 0.6 V with a scan rate of 0.1 V/s. Electrochemical impedance spectroscopy (EIS) measurements were performed for characterizing the electrode modification with a 5 mM solution of 1:1 ferro/ferricyanide containing 0.1 M KCl. EIS were conducted at a potential bias of 0.2 V within a frequency range from 0.1 Hz to 10^5 Hz with an amplitude of 5 mV.

3. Results and Discussion

3.1. Principle of the Developed Sensor

The electrochemical sensing platform was constructed by immobilizing Lac aptamers modified with thiol group and redox tag ferrocene (Fc) onto a gold electrode through Au-S covalent interactions, forming a stable self-assembled monolayer (SAM). To minimize nonspecific adsorption, the electrode was subsequently treated with MCH, which blocks the unoccupied regions of the gold surface. As illustrated in Scheme 1A, the single-stranded Lac201 (ssLac201) probe adopts a flexible conformation in the absence of Lac and the terminal Fc tag remains relatively distant from the electrode surface, resulting in slow electron-transfer efficiency. In the presence of Lac, the target molecule specifically binds to the aptamer probe, triggering a conformational rearrangement and forming a stem-loop structure. This structural transition drives the Fc tag closer to the electrode surface, thereby facilitating fast electron-transfer and producing an increase in the redox current

signal. To further improve the sensing performance, a double-stranded Lac201 (dsLac201) aptamer probe was designed (Scheme 1B). The immobilized aptamer hybridizes with a short complementary DNA (cDNA) strand to form a rigid duplex structure. Compared with the flexible ssLac201 probe, the dsLac201 configuration provides a more defined spatial orientation, which positions the Fc reporter further away from the electrode surface in the absence of the target. While in the presence of Lac, the specific aptamer–target binding breaks the duplex structure and induces a strand displacement process. This process leads to the rearrangement of the aptamer conformational and brings the Fc tag closer to the electrode interface, thereby increasing the electron-transfer efficiency and the detected Faradic current. The utilization of the dsLac201 strategy reduced the background current and lead to a larger conformational change upon target binding, thus enhancing the signal-to-noise ratio and detection sensitivity of the proposed sensor [31].

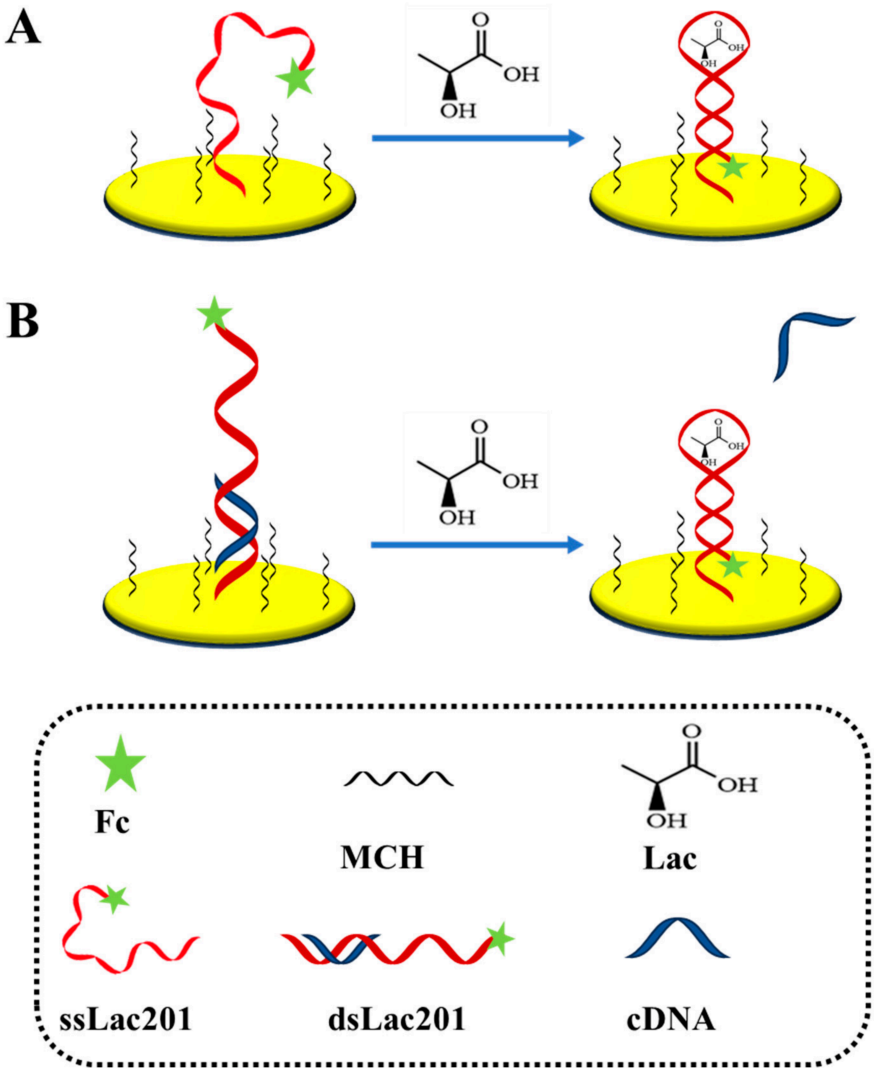

Scheme 1. E-AB sensor for detection of Lac with (**A**) single-stranded probe (ssLac201) and (**B**) double-stranded probe (dsLac201).

3.2. Comparison of Electrochemical Responses of ssLac201 and dsLac201

To compare the sensing performance of different probe architectures for Lac detection, the electrochemical responses of ssLac201 and dsLac201 were investigated by DPV. The relative increased Fc Faraday current was recorded as the sensor signal according to $(I - I_0)/I_0$ (%), where I and I_0 are peak currents from the terminal redox molecule of the aptamer with and without target binding, respectively. As illustrated in Figure 1A,B, both

probes generated enhanced peak currents after incubation with 10 mM Lac, indicating that target binding effectively triggered a "signal-on" electrochemical response. However, the magnitude of the current increase was significantly dependent on probe configuration. In particular, the relative current increase reached 106% for ssLac201, whereas dsLac201 achieved a much higher increase of 179%. This improvement is likely due to the rigid duplex conformation of dsLac201, which positions the Fc reporter farther from the electrode surface in the absence of target. After Lac binding, the resulting structural rearrangement produces a larger distance-dependent electron-transfer change, thereby generating a stronger electrochemical response. To further investigate the electrochemical behavior of the dsLac201 sensing interface after Lac recognition, CV was performed at different scan rates and a linear relationship between the anodic peak current and scan rates was obtained (Figure S1). This observation suggests that the redox process of the target-bound Fc-labeled aptamer probe is surface-confined, confirming that the electrochemical signal originates from the immobilized aptamer–target complex rather than from diffusing electroactive species in solution. Therefore, the dsLac201 probe design was selected as the optimal sensing configuration for subsequent experiments and for the construction of the dual-target logic-gated sensing platform.

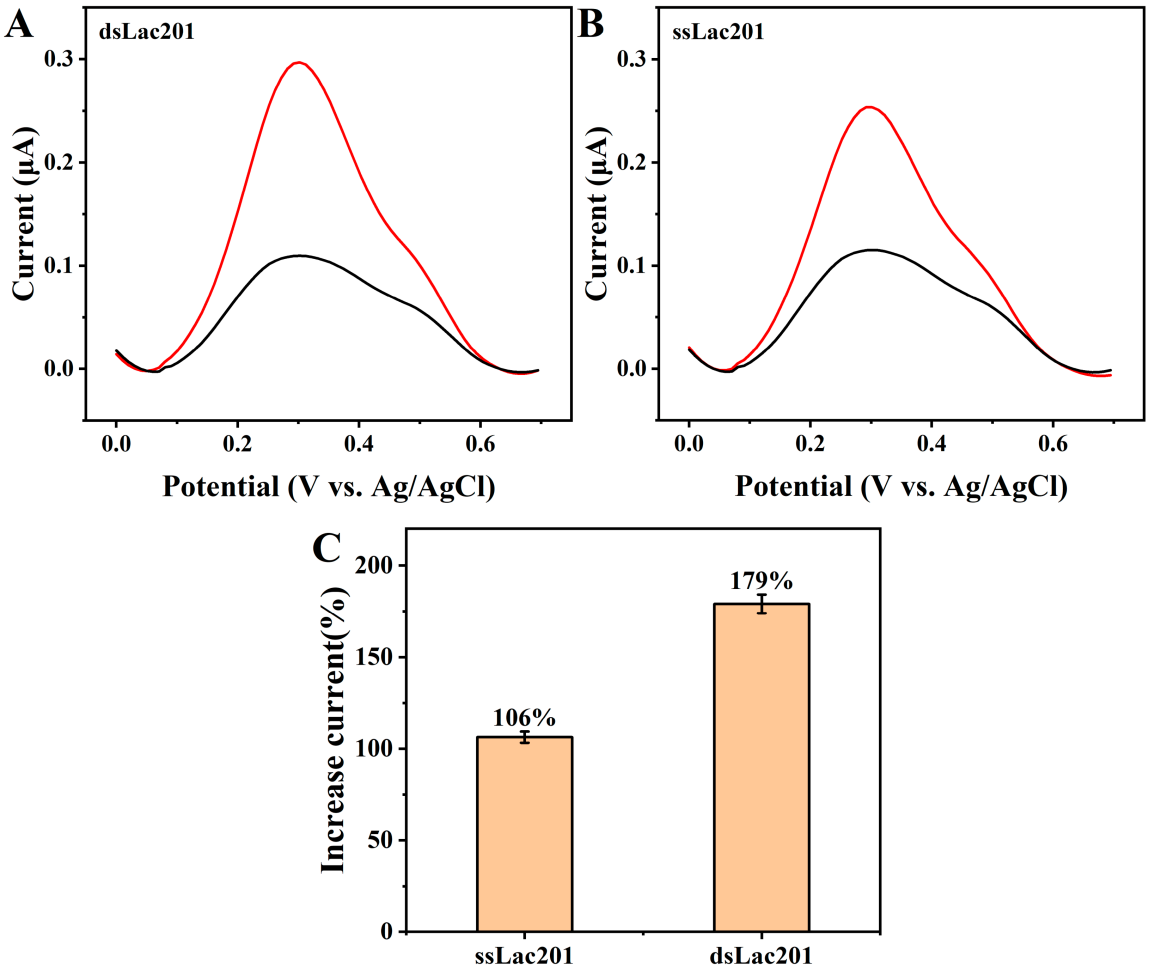

Figure 1. The DPV curves of the dsLac201 (**A**) and ssLac201 (**B**) probes for 10 mM L-Lac addition (black: without target; red: with target). (**C**) The calculated increase in current signal of different probes after target binding.

3.3. Optimization of Experimental Conditions

To maximize the analytical performance of the dsLac201-based sensor, key experimental parameters affecting probe immobilization and target recognition were systematically optimized, including probe concentration, target incubation time, and incubation temperature. Since the target-induced structural rearrangement of the double-stranded probe directly governs the electron transfer of the Fc reporter, the surface density of the immobilized probes plays critical roles in determining both the background current and the target-binding induced signal change. As shown in Figure 2A, the effect of probe concentration on the signal response of dsLac201 sensor was investigated. The relative current response increased progressively as the probe concentration was raised from 0.05 to 0.5 μM, reaching a maximum at 0.5 μM. This result suggests that an appropriate increase in probe density enhances the number of effective recognition sites and improves the sensor signal. However, when the probe concentration was further increased beyond 0.5 μM, the signal response decreased. The reason can be attributed to the dense aptamer packing on the surface with high aptamer concentrations, which can restrict the conformational change for target binding due to the electrostatic repulsion between adjacent nucleic acid probes and increased steric hindrance. Therefore, 0.5 μM was selected as the optimal probe concentration for subsequent experiments.

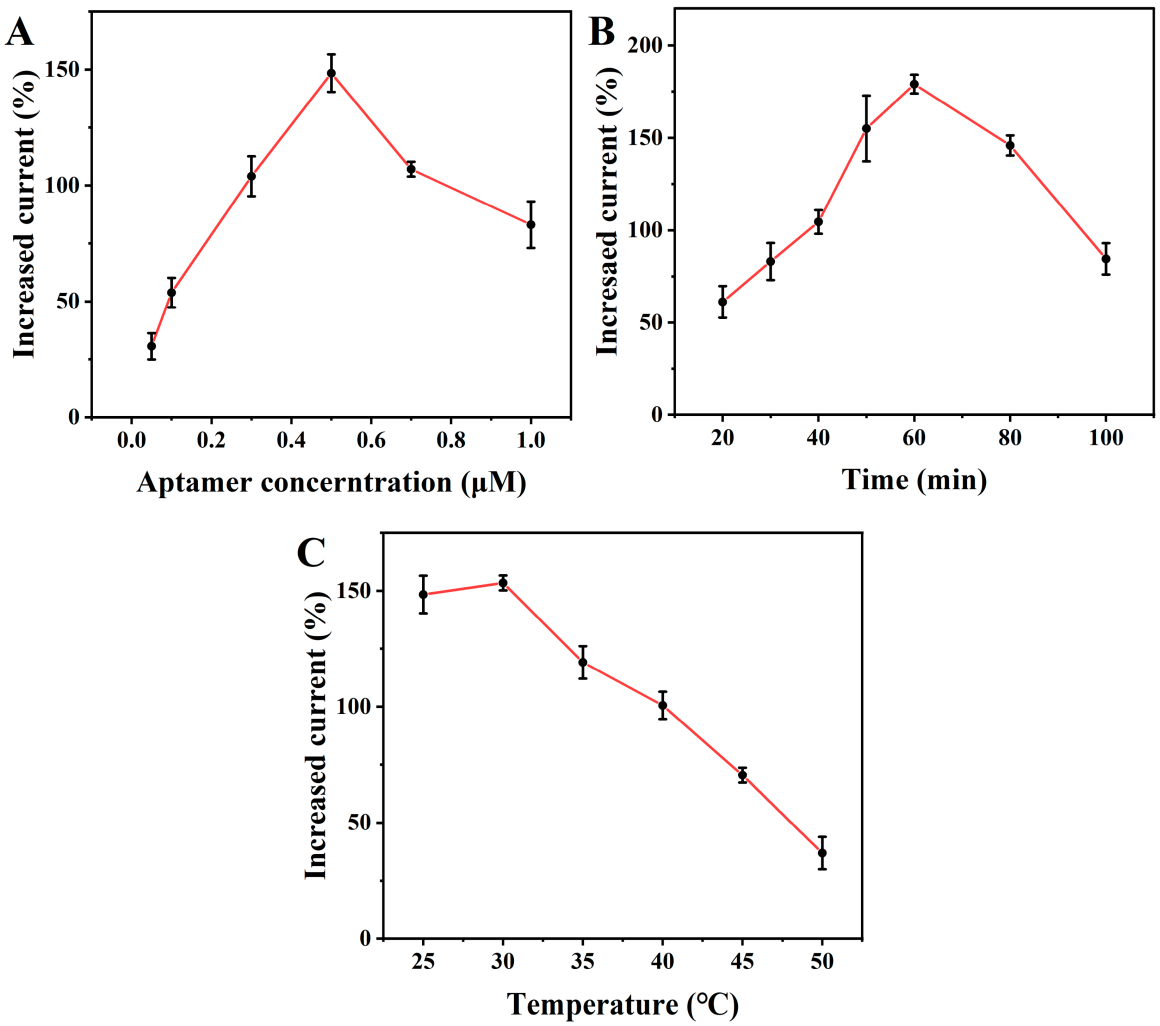

Figure 2. Optimization of experimental parameters for E-AB sensor fabrication with dsLac20 probe. (**A**) Aptamer concentration; (**B**) Analyte incubation time; (**C**) Incubation temperature.

The incubation time for target recognition was subsequently optimized over the range of 20 to 100 min (Figure 2B). The signal response increased steadily with increasing incubation time from 20 to 60 min, indicating gradual formation of the aptamer–target complex and more dsLac201 probe with conformational change. A maximum response was obtained at 60 min. When the incubation time was further extended beyond 60 min, the signal gradually decreased. This decline may be associated with reduced structural stability of the aptamer interface during prolonged incubation, which weakens the signal transduction efficiency. Thus, 60 min was chosen as the optimal incubation time.

The effect of incubation temperature on sensor performance was also evaluated (Figure 2C). The signal response remained high and relatively stable within the 25 to 30 °C range, indicating that the aptamer maintained favorable conformational stability and binding activity under near-room-temperature conditions. In contrast, when the temperature exceeded 30 °C, the signal response decreased gradually with increasing temperature. This behavior may be attributed to reduced stability of the duplex probe structure and disruption in the target-induced aptamer conformation at high temperatures, which further affects the distance modulation between Fc and electrode surface. Based on these results, the optimized experimental conditions for subsequent measurements were determined to be 0.5 μM probe concentration and 60 min target incubation time at room-temperature.

3.4. Analytical Performance of the dsLac201 Sensor

To evaluate the analytical performance of the dsLac201-based electrochemical sensor, DPV measurements were performed by detecting a series of Lac concentrations (Figure 3A). As the concentration increased, the DPV peak current gradually increased, indicating a concentration-dependent "signal-on" response. This behavior is attributed to the target-induced destabilization and conformational rearrangement of the double-stranded probe, followed by specific binding of the aptamer to Lac, which drives the Fc close to the electrode surface and facilitate fast electron transfer.

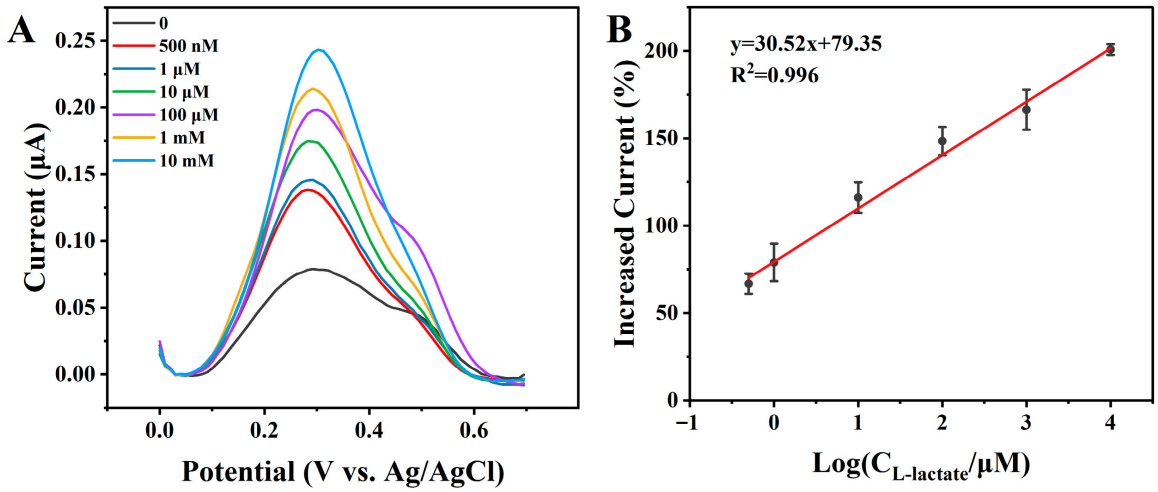

Figure 3. (**A**) DPV responses of the sensor toward different concentrations of Lac; (**B**) Calibration curve showing the relationship between the response signal and the logarithm of Lac concentration.

A good linear relationship was obtained between the response signal and the logarithm of Lac concentration over the range of 500 nM to 10 mM, with the calibration equation $y = 30.52x + 79.35$ and a correlation coefficient of $R^2 = 0.996$. The limit of detection (LOD) was calculated to be 157 nM based on the 3σ rule (where σ is the standard deviation of the blank). These results demonstrate that the proposed sensor exhibits high sensitivity, a broad linear range, and a low detection limit for Lac detection. Notably, the linear detection

range covers both physiological Lac levels and the elevated concentrations associated with pathological metabolic dysregulation, highlighting its feasibility for clinically relevant analysis. Furthermore, comparison with previously reported Lac sensing methods indicates that the sensor developed in this work provides competitive analytical performance, while offering the additional advantages of a simplified sensing architecture and straightforward operation (Table S1) [32–41]. These characteristics demonstrate the potential of the proposed platform for biomedical analysis and prostate cancer-related metabolic monitoring.

To investigate the selectivity of the proposed dsLac201-based electrochemical sensor, interference studies were performed using Lac and several potentially coexisting small molecules, including D-lactate, glucose, glycine, L-alanine, L-cysteine, and acetic acid. As shown in Figure 4, the sensor produced a distinct and significantly higher response toward 10 μM L-Lac compared with all tested interferences. Notably, only negligible signal changes were observed for the non-target molecules, even when each interference was present at 1 mM, corresponding to a 100-fold high relative to L-lactate. Although a slight signal response was observed for glucose at a high concentration, the response was significantly lower than that of Lac. The minor interference may arise from nonspecific adsorption at the electrode interface under high glucose concentrations. In practical applications, such interference can be minimized by sample dilution or antifouling surface modification [23,42]. In particular, D-Lac, the stereoisomer of L-Lac, induced only a weak response, indicating that the aptamer probe possesses excellent stereoselective recognition capability. These results demonstrate that the proposed sensor exhibits high selectivity and strong anti-interference performance for accurate L-Lac determination.

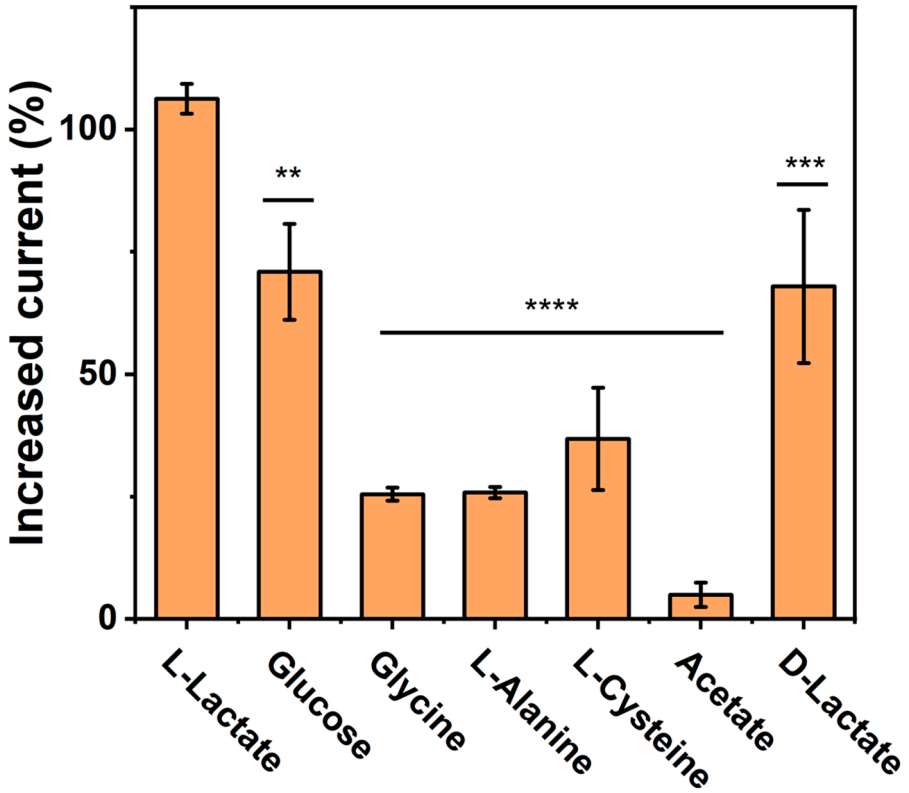

Figure 4. Selectivity of the dsLac201-based L-Lac sensor (** $p < 0.01$, *** $p < 0.005$, **** $p < 0.001$).

3.5. Construction of an AND Logic-Gated Dual-Target Sensor

Aptamers are highly programmable nucleic acid recognition elements that can be rationally engineered to achieve target induced structural switching and logic-gated signal transduction through sequence design [43]. Based on the optimized dsLac201 sensing

configuration, we further designed the Lac aptamer by extending nine nucleotides at the 5′ end to enable partial complementary hybridization with the PSA aptamer, thereby constructing a dual-input electrochemical AND logic gate for the simultaneous recognition of L-Lac and PSA (Scheme 2). In this design, L-Lac and PSA function as the two logic inputs, while the DPV current signal serves as the output. As illustrated in Scheme 2, the presence of either target alone induces only limited structural rearrangement of the hybridized probe, resulting in a relatively weak signal response. In contrast, when L-Lac and PSA present simultaneously, dual target recognition triggers completely dissociation of the two aptamers assembly, which produces a significantly enhanced electrochemical current signal. Thus, the dual-input state generates a stronger output than either single-input condition, consistent with the operational behavior of an AND logic gate. To verify the feasibility of this dual-target sensing strategy, comparative electrochemical measurements were performed using L-Lac alone, PSA alone, and a mixture of L-Lac and PSA. The simultaneous presence of both analytes produced the highest signal response, with the current increasing by 87.8%, whereas L-Lac alone and PSA alone yielded lower current increases of 40.0% and 28.0%, respectively (Figure 5). These results confirm the successful construction of the AND logic-gated electrochemical sensing platform and demonstrate its capability for dual targets sensing signal output, providing a promising strategy for more accurate PC-related biomarker analysis.

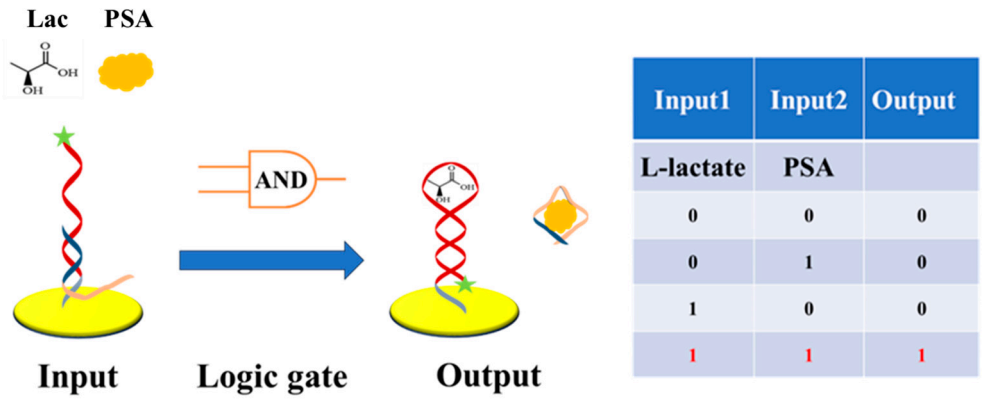

Input1	Input2	Output
L-lactate	PSA	
0	0	0
0	1	0
1	0	0
1	1	1

Scheme 2. Schematic illustration of the AND logic-gated electrochemical sensing strategy for dual recognition of L-Lac and PSA.

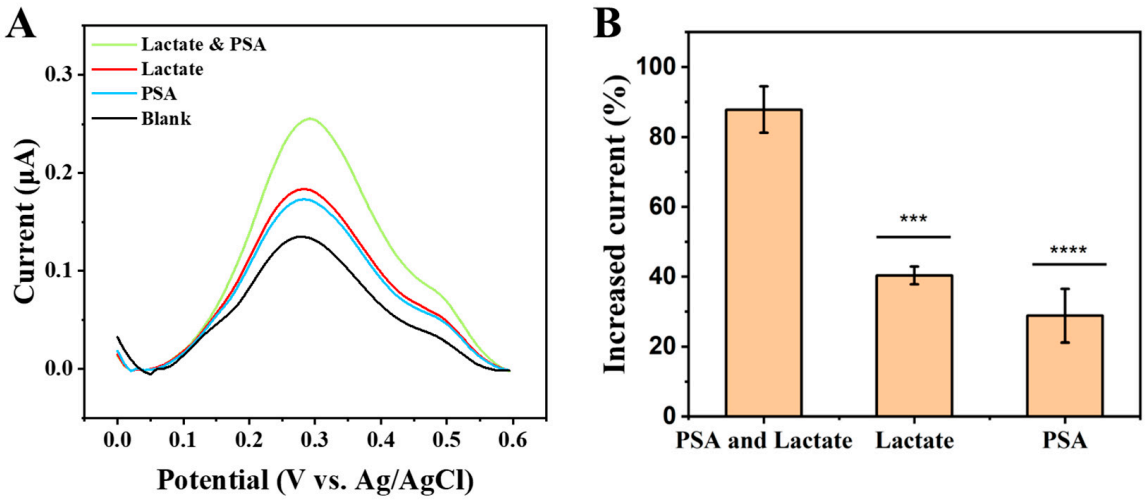

Figure 5. (**A**) DPV curves in response to dual target L-Lac and PSA, L-Lac alone, and PSA alone and (**B**) the corresponding calculated current changes (*** $p < 0.005$, **** $p < 0.001$).

To further characterize the stepwise fabrication of the sensing interface and verify the proposed dual-target triggered structural change, EIS was employed to monitor changes in the interfacial charge transfer resistance (R_{ct}) at each modification stage and under different target-input conditions (Figure 6). The bare AuE show a relatively low R_{ct}, reflecting the facile electron transfer at the clean gold surface (curve a). After immobilization of the double stranded probe, the R_{ct} increased markedly due to the formation of a negatively charged DNA layer that hinders the interfacial electron transfer process (curve b). Following treatment with MCH, the impedance further increased, indicating successful backfilling of the unoccupied gold surface and formation of a more compact and well-organized self-assembled monolayer (curve c). The addition of L-Lac alone caused only a slight change in the R_{ct}, indicating that although L-Lac may induce a limited conformational response, it does not cause substantial disruption of the surface-confined nucleic acid assembly under this dual-target configuration (curve d). Upon exposure to PSA, the R_{ct} increased significantly, suggesting the formation of a more electrically insulated interfacial layer (curve e). This observation indicates that PSA-aptamer binding alone does not trigger complete dissociation of the double strand structure and the hybridized structure remained largely preserved. When L-Lac was then introduced into the PSA-bound system, a pronounced decrease in R_{ct} was observed (curve f). This decrease suggests that the dual recognition of targets induced a larger structural rearrangement of the nucleic acid complex, leading to reduced steric hindrance and improved interfacial electron transfer. To further verify the specificity of the dual-aptamer sensing mechanism, the PSA aptamer was replaced with an ATP aptamer as a non-binding control (Figure S2). Under the same dual-target conditions, no significant DPV or EIS signal changes were observed upon addition of L-Lac and PSA, confirming that the observed responses arise from the specific interactions of the dual-aptamer assembly and provide strong support for the proposed AND logic-gated signal transduction mechanism.

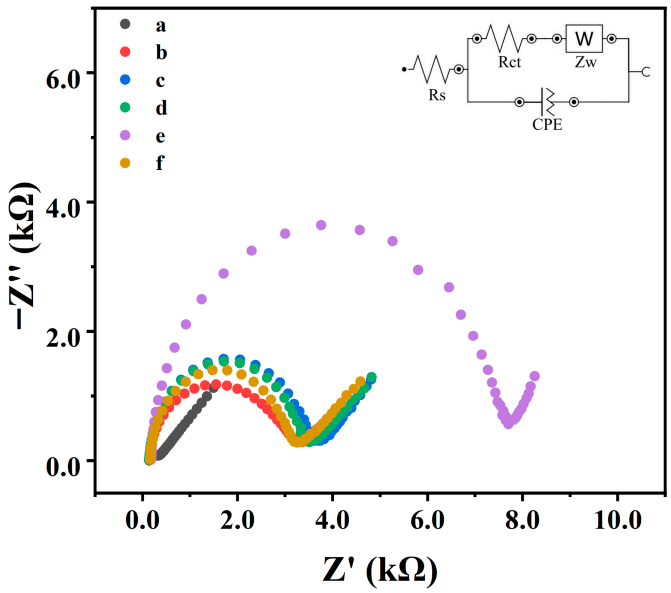

Figure 6. Nyquist plots recorded for (a) bare AuE, (b) double stranded aptamers modified AuE, (c) MCH-blocked AuE, (d) L-Lac, (e) PSA, and (f) L-Lac and PSA.

3.6. Real Sample Analysis

To further assess the practical applicability of the proposed dual-target E-AB sensor in complex biological matrices, fetal bovine serum (FBS) was diluted 10-fold with HEPES buffer, and different concentrations of L-Lac or PSA were spiked into the diluted serum to test the sensor performance. As shown in Figure 7, the sensor maintained promising

analytical performance in the serum solutions, demonstrating excellent resistance to matrix interference. When the concentration of PSA was fixed at 4 ng mL^{-1}, the sensor response exhibited a linear relationship with the logarithm of L-Lac concentration over the range of 500 nM to 10 mM, with the calibration equation y = 27.3x + 44.6 and a correlation coefficient of R^2 = 0.997. Conversely, when the concentration of L-Lac was fixed at 1 mM, a linear response toward PSA was obtained in the range of 10 pg mL^{-1} to 500 ng mL^{-1}, with the calibration equation y = 40.59x + 99.20 and R^2 = 0.991. These results indicate that the proposed sensing platform maintains reliable dual-analyte quantification capability in a complex serum matrix.

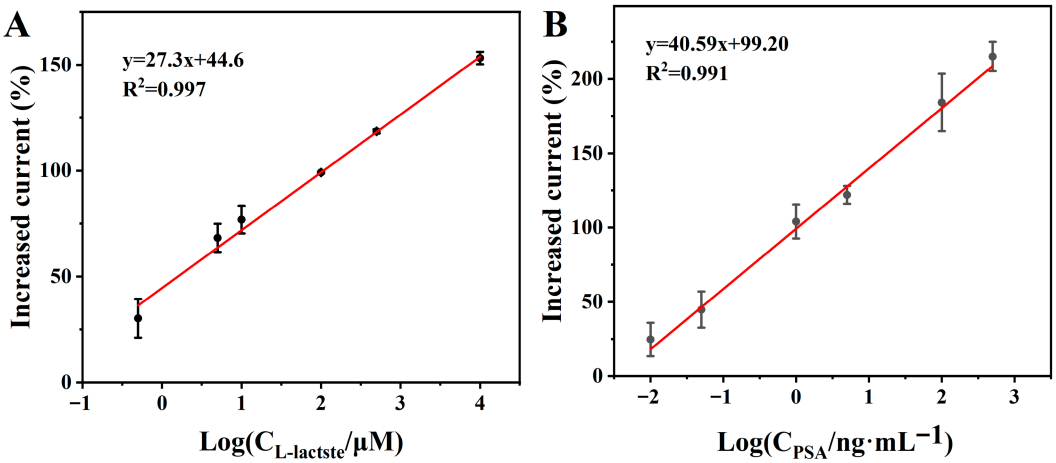

Figure 7. Linear relationship of target analyte detection concentration in 10% FBS samples. (**A**) L-Lac; (**B**) PSA.

To further evaluate analytical accuracy, recovery experiments were carried out for PSA in spiked FBS and human serum samples by the standard addition method (Tables 2 and 3) in the presence of 1 mM L-Lac. The recoveries in spiked FBS samples ranged from 98.8% to 109.0%, with relative standard deviations (RSDs) of 1.37% to 2.62%, while in human serum samples ranged from 84.2% to 110% with RSDs below 10%, indicating great accuracy and reproducibility. Overall, these findings demonstrate that the proposed sensor enables for simultaneous L-Lac and PSA analysis in real samples, highlighting its potential for practical biomedical applications and prostate cancer-related biomarker monitoring.

Table 2. The recovery experiments of the sensor for PSA in 10% FBS.

Number	Add PSA (ng/mL)	Detected PSA (ng/mL)	Recovery (%)	RSD (%)
1	0.1	0.109	109	2.62
2	4	3.95	98.8	1.37
3	50	53.1	106	2.27

Table 3. The recovery experiments of the sensor for PSA in 10% human serum.

Number	Add PSA (ng/mL)	Detected PSA (ng/mL)	Recovery (%)	RSD (%)
1	0.1	0.11	110	1.11
2	4	3.80	95	4.52
3	50	42.1	84.2	9.33

4. Conclusions

In this work, we developed a novel, simple, and sensitive E-AB sensor for the dual-target detection of L-Lac and PSA. By comparing two sensing configurations based on the single-stranded and double-stranded forms of the Lac aptamer, the double-stranded probe architecture was identified as the optimal design owing to its improved signal response and reduced background current. After optimization of key experimental parameters, including probe concentration, incubation time, and temperature, the developed sensor exhibited high sensitivity toward L-Lac, with a LOD of 157 nM, a wide linear range of 500 nM to 10 mM, and excellent selectivity.

Based on this optimized platform, a dual-aptamer sensing interface was further constructed through rational nucleic acid design, enabling the simultaneous electrochemical detection of L-Lac and PSA. The dual-target sensor exhibited broad dynamic ranges for both analytes (L-Lac: 500 nM–10 mM; PSA: 10 pg mL^{-1}–500 ng mL^{-1}) and maintained promising analytical performance in serum samples, demonstrating good accuracy, reproducibility, and anti-interference capability. Overall, this work provides a simple strategy for multiplex electrochemical biosensing and offers potential for PC biomarker monitoring and clinical treatment evaluation.

Supplementary Materials: The following supporting information can be downloaded at: https://www.mdpi.com/article/10.3390/targets4020015/s1, Figure S1. (A) CV curves at different scan rates; (B) The relationship between anodic peak current and scan rates. Figure S2. (A) DPV and (B) EIS curves by using an ATP aptamer as a non-binding control for the dual-aptamer assembly. Table S1. Comparison of this work with other reported L-Lac sensors.

Author Contributions: Conceptualization, Z.H. and L.F.; methodology, Z.H. and X.Z.; validation, Z.H., X.Z. and H.S.; investigation, Z.H. and X.Z.; resources, L.F.; writing—original draft preparation, Z.H. and X.Z.; writing—review and editing, F.W., Z.L. and L.F.; supervision, Z.L. and L.F.; funding acquisition, Z.L. and L.F. All authors have read and agreed to the published version of the manuscript.

Funding: This research was funded by the National Natural Science Foundation of China (No. 21705106), the National Natural Science Foundation of China (No. 22177067), Advanced Materials-National Science and Technology Major Project (No. 2025ZD0619502, No. 2025ZD0620100) and Shanghai Sailing Program (No. 24YF2712500).

Institutional Review Board Statement: Not applicable.

Informed Consent Statement: Not applicable.

Data Availability Statement: Data will be made available on request.

Conflicts of Interest: The authors declare no conflicts of interest.

References

1. Pinsky Paul, F.; Parnes, H. Screening for Prostate Cancer. *N. Engl. J. Med.* **2023**, *388*, 1405–1414. [CrossRef]
2. Soeterik, T.F.W.; Wu, X.; Van den Bergh, R.C.N.; Kesch, C.; Zattoni, F.; Falagario, U.; Martini, A.; Miszczyk, M.; Fasulo, V.; Maggi, M.; et al. Personalised Prostate Cancer Diagnosis: Evaluating Biomarker-based Approaches to Reduce Unnecessary Magnetic Resonance Imaging and Biopsy Procedures. *Eur. Urol. Open Sci.* **2025**, *75*, 106–119. [CrossRef] [PubMed]
3. Hamed, N.W.; Elbeljihy, H.S.; Hussin, S.A.; Fouda, R.M.; Oy, E.-K.; Magar, R.W. From prostate specific antigen to genomic signatures: Advances in biomarkers for prostate cancer diagnosis and prognosis. *Transl. Oncol.* **2026**, *66*, 102719. [CrossRef]
4. Daryanto, B.; Trianto, R.; Seputra, K.P.; Purnomo, A.F. Evaluation of Cutoff Point Prostate Specific Antigen (PSA) and Prostate Specific Antigen Density (PSAD) in Patients with Suspected Prostate Cancer. *Med. Arch.* **2024**, *78*, 12–15. [CrossRef]
5. Armbruster, D.A. Prostate-specific antigen: Biochemistry, analytical methods, and clinical application. *Clin. Chem.* **1993**, *39*, 181–195. [CrossRef]
6. Ibau, C.; Md Arshad, M.K.; Gopinath, S.C.B. Current advances and future visions on bioelectronic immunosensing for prostate-specific antigen. *Biosens. Bioelectron.* **2017**, *98*, 267–284. [CrossRef]

7. Özyurt, C.; Uludağ, İ.; İnce, B.; Sezgintürk, M.K. Biosensing strategies for diagnosis of prostate specific antigen. *J. Pharm. Biomed. Anal.* **2022**, *209*, 114535. [CrossRef] [PubMed]
8. Gonzales, J.C.; Fink, L.M.; Goodman, O.B.; Symanowski, J.T.; Vogelzang, N.J.; Ward, D.C. Comparison of Circulating MicroRNA 141 to Circulating Tumor Cells, Lactate Dehydrogenase, and Prostate-Specific Antigen for Determining Treatment Response in Patients With Metastatic Prostate Cancer. *Clin. Genitourin. Cancer* **2011**, *9*, 39–45. [CrossRef] [PubMed]
9. Mori, K.; Kimura, S.; Parizi, M.K.; Enikeev, D.V.; Glybochko, P.V.; Seebacher, V.; Fajkovic, H.; Mostafaei, H.; Lysenko, I.; Janisch, F.; et al. Prognostic Value of Lactate Dehydrogenase in Metastatic Prostate Cancer: A Systematic Review and Meta-analysis. *Clin. Genitourin. Cancer* **2019**, *17*, 409–418. [CrossRef]
10. Huang, P.-J.J.; Liu, J. Simultaneous Detection of L-Lactate and D-Glucose Using DNA Aptamers in Human Blood Serum. *Angew. Chem. Int. Ed.* **2023**, *62*, e202212879. [CrossRef]
11. Tessem, M.B.; Swanson, M.G.; Keshari, K.R.; Albers, M.J.; Joun, D.; Tabatabai, Z.L.; Simko, J.P.; Shinohara, K.; Nelson, S.J.; Vigneron, D.B.; et al. Evaluation of lactate and alanine as metabolic biomarkers of prostate cancer using 1H HR-MAS spectroscopy of biopsy tissues. *Magn. Reson. Med.* **2008**, *60*, 510–516. [CrossRef] [PubMed]
12. Chetta, P.; Sriram, R.; Zadra, G. Lactate as Key Metabolite in Prostate Cancer Progression: What Are the Clinical Implications? *Cancers* **2023**, *15*, 3474. [CrossRef]
13. van der Mijn, J.C.; Kuiper, M.J.; Siegert, C.E.H.; Wassenaar, A.E.; van Noesel, C.J.M.; Ogilvie, A.C. Lactic Acidosis in Prostate Cancer: Consider the Warburg Effect. *Case Rep. Oncol.* **2017**, *10*, 1085–1091. [CrossRef]
14. Biagi, S.; Ghimenti, S.; Onor, M.; Bramanti, E. Simultaneous determination of lactate and pyruvate in human sweat using reversed-phase high-performance liquid chromatography: A noninvasive approach. *Biomed. Chromatogr.* **2012**, *26*, 1408–1415. [CrossRef]
15. Arrieta, M.P.; Parres, F.; López, J.; Jiménez, A. Development of a novel pyrolysis-gas chromatography/mass spectrometry method for the analysis of poly(lactic acid) thermal degradation products. *J. Anal. Appl. Pyrolysis* **2013**, *101*, 150–155. [CrossRef]
16. Moukri, N.; Patella, B.; Inguanta, R. Recent progress in low-cost methods for electrochemical sensor fabrication. *Curr. Opin. Electrochem.* **2025**, *54*, 101771. [CrossRef]
17. Kumar, N.; Alvarez, N.T. Electrochemical sensors for prostate, lung, breast, and colon cancer biomarkers: A review. *J. Electroanal. Chem.* **2026**, *1001*, 119695. [CrossRef]
18. Zhu, M.; Zeng, X.; Yue, T.; Gao, X.; Liang, Q.; Li, B.; Li, S.; Li, H.; Xia, F. Toward point-of-care testing: The emerging role of electrochemical aptamer-based biosensors. *J. Electroanal. Chem.* **2026**, *1010*, 120023. [CrossRef]
19. Stangherlin, S.; Lui, N.; Lee, J.H.; Liu, J. Aptamer-based biosensors: From SELEX to biomedical diagnostics. *TrAC Trends Anal. Chem.* **2025**, *191*, 118349. [CrossRef]
20. Lukman, Y.; Shamsuddin, S.H. Advances in aptamer-based biosensors for cancer biomarker detection: A systematic review of emerging technologies and translational potential. *Microchem. J.* **2026**, *221*, 116787. [CrossRef]
21. Majdinasab, M.; Marty, J.L. Recent advances in electrochemical aptasensors for detection of biomarkers. *Pharmaceuticals* **2022**, *15*, 995. [CrossRef]
22. Sun, D.; Luo, Z.; Lu, J.; Zhang, S.; Che, T.; Chen, Z.; Zhang, L. Electrochemical dual-aptamer-based biosensor for nonenzymatic detection of cardiac troponin I by nanohybrid electrocatalysts labeling combined with DNA nanotetrahedron structure. *Biosens. Bioelectron.* **2019**, *134*, 49–56. [CrossRef]
23. Hu, Z.; Zhu, R.; Figueroa-Miranda, G.; Zhou, L.; Feng, L.; Offenhäusser, A.; Mayer, D. Truncated Electrochemical Aptasensor with Enhanced Antifouling Capability for Highly Sensitive Serotonin Detection. *Biosensors* **2023**, *13*, 881. [CrossRef]
24. Zhao, B.; Miao, P.; Hu, Z.; Zhang, X.; Geng, X.; Chen, Y.; Feng, L. Signal-on electrochemical aptasensors with different target-induced conformations for prostate specific antigen detection. *Anal. Chim. Acta* **2021**, *1152*, 338282. [CrossRef] [PubMed]
25. Hu, Z.; Zhu, R.; Figueroa-Miranda, G.; Feng, L.; Offenhäusser, A.; Mayer, D. Potential-pulse-assisted co-immobilization of multiple aptamers on microelectrode arrays for multiplexed neurotransmitter detection. *Biosens. Bioelectron.* **2025**, *290*, 117992. [CrossRef] [PubMed]
26. Zhou, L.; Figueroa-Miranda, G.; Chen, S.; Neis, M.; Hu, Z.; Zhu, R.; Li, Y.; Prömpers, M.; Offenhäusser, A.; Mayer, D. Flexible Multielectrode Arrays Based Electrochemical Aptasensor for Glycated Human Serum Albumin Detection. *SSRN Electron. J.* **2023**, *386*, 133730. [CrossRef]
27. Ma, Y.; Zhang, H.; Shen, X.; Yang, X.; Deng, Y.; Tian, Y.; Chen, Z.; Pan, Y.; Luo, H.; Zhong, C.; et al. Aptamer functionalized hypoxia-potentiating agent and hypoxia-inducible factor inhibitor combined with hypoxia-activated prodrug for enhanced tumor therapy. *Cancer Lett.* **2024**, *598*, 217102. [CrossRef]
28. Amu, G.; Zhang, G.; Jing, N.; Ma, Y. Developing Stapled Aptamers with a Constrained Conformation for Osteogenesis Imperfect Therapeutics. *J. Med. Chem.* **2024**, *67*, 18883–18894. [CrossRef]
29. Savory, N.; Abe, K.; Sode, K.; Ikebukuro, K. Selection of DNA aptamer against prostate specific antigen using a genetic algorithm and application to sensing. *Biosens. Bioelectron.* **2010**, *26*, 1386–1391. [CrossRef]

30. Xiao, Y.; Lai, R.Y.; Plaxco, K.W. Preparation of electrode-immobilized, redox-modified oligonucleotides for electrochemical DNA and aptamer-based sensing. *Nat. Protoc.* **2007**, *2*, 2875–2880. [CrossRef]
31. Zhou, L.; Zhu, R.; Figueroa-Miranda, G.; Neis, M.; Offenhäusser, A.; Mayer, D. Ratiometric electrochemical aptasensor with strand displacement for insulin detection in blood samples. *Anal. Chim. Acta* **2024**, *1317*, 342823. [CrossRef]
32. Figueroa-Miranda, G.; Wu, C.; Zhang, Y.; Nörbel, L.; Lo, Y.; Tanner, J.A.; Elling, L.; Offenhäusser, A.; Mayer, D. Polyethylene glycol-mediated blocking and monolayer morphology of an electrochemical aptasensor for malaria biomarker detection in human serum. *Bioelectrochemistry* **2020**, *136*, 107589. [CrossRef]
33. Feng, L.; Lyu, Z.; Offenhäusser, A.; Mayer, D. Multi-Level Logic Gate Operation Based on Amplified Aptasensor Performance. *Angew. Chem. Int. Ed.* **2015**, *54*, 7693–7697. [CrossRef] [PubMed]
34. Weng, X.; Li, M.; Chen, L.; Peng, B.; Jiang, H. A Wearable Nanozyme–Enzyme Electrochemical Biosensor for Sweat Lactate Monitoring. *Talanta* **2024**, *279*, 126675. [CrossRef] [PubMed]
35. Wang, R.; Zhai, Q.; An, T.; Gong, S.; Cheng, W. Stretchable Gold Fiber-Based Wearable Textile Electrochemical Biosensor for Lactate Monitoring in Sweat. *Talanta* **2021**, *222*, 121484. [CrossRef] [PubMed]
36. Khan, A.; Winder, M.; Hossain, G. Modified Graphene-Based Nanocomposite Material for Smart Textile Biosensor to Detect Lactate from Human Sweat. *Biosens. Bioelectron. X* **2022**, *10*, 100103. [CrossRef]
37. Minamiki, T.; Tokito, S.; Minami, T. Fabrication of a Flexible Biosensor Based on an Organic Field-Effect Transistor for Lactate Detection. *Anal. Sci.* **2019**, *35*, 103–106. [CrossRef]
38. Shitanda, I.; Mitsumoto, M.; Loew, N.; Yoshihara, Y.; Watanabe, H.; Mikawa, T.; Tsujimura, S.; Itagaki, M.; Motosuke, M. Continuous Sweat Lactate Monitoring System with Integrated Screen-Printed MgO-Templated Carbon–Lactate Oxidase Biosensor and Microfluidic Sweat Collector. *Electrochim. Acta* **2021**, *368*, 137620. [CrossRef]
39. Choi, Y.M.; Lim, H.; Lee, H.-N.; Park, Y.M.; Park, J.-S.; Kim, H.-J. Selective Nonenzymatic Amperometric Detection of Lactic Acid in Human Sweat Utilizing a Multi-Walled Carbon Nanotube–Polypyrrole Core–Shell Nanowire. *Biosensors* **2020**, *10*, 111. [CrossRef]
40. Xuan, X.; Pérez-Ràfols, C.; Chen, C.; Cuartero, M.; Crespo, G.A. Lactate Biosensing for Reliable On-Body Sweat Analysis. *ACS Sens.* **2021**, *6*, 2763–2771. [CrossRef]
41. Madden, J.; Vaughan, E.; Thompson, M.; O'Riordan, A.; Galvin, P.; Iacopino, D.; Rodrigues Teixeira, S. Electrochemical Sensor for Enzymatic Lactate Detection Based on Laser-Scribed Graphitic Carbon Modified with Platinum, Chitosan, and Lactate Oxidase. *Talanta* **2022**, *246*, 123492. [CrossRef] [PubMed]
42. Zhao, C.; Li, X.; Wu, Q.; Liu, X. A Thread-Based Wearable Sweat Nanobiosensor. *Biosens. Bioelectron.* **2021**, *188*, 113270. [CrossRef] [PubMed]
43. Garland, N.T.; Schmieder, J.; Johnson, Z.T.; Hjort, R.G.; Chen, B.; Andersen, C.; Sanborn, D.; Kjeldgaard, G.; Pola, C.C.; Li, J.; et al. Wearable Flexible Perspiration Biosensors Using Laser-Induced Graphene and Polymeric Tape Microfluidics. *ACS Appl. Mater. Interfaces* **2023**, *15*, 38201–38213. [CrossRef] [PubMed]